Wireless transfer between antenna arrays at the Talbot distance

Rudolf Sprik*
van der Waals-Zeeman Instituut, Universiteit van Amsterdam, Valckenierstraat 65, 1018 XE Amsterdam, The Netherlands
(Received 5 January 2005; revised manuscript received 19 April 2005; published 14 September 2005)

In modern multiple input multiple output (MIMO) wireless communication systems arrays of antennas are employed to enhance the data transfer rate. Scattering of the waves in the medium between the antennas can actually enhance the transfer capacity by decorrelating the available channels. Here it is shown that the transfer capacity between arrays of regularly spaced antennas depends intricately on the distance between the arrays and on the arrangement of scatterers. The relevant length scale is the Talbot distance $L_{\mathrm{Talbot}}=2d^2/\lambda$ known from optics as the distance where the self-imaging occurs of coherently illuminated gratings with d the grating period and λ the wavelength. The modulation of singular values of the channel transfer matrix occurs at fractions of L_{Talbot}.

DOI: 10.1103/PhysRevE.72.037602 PACS number(s): 41.20.Jb, 84.40.Ua, 42.25.Bs

To enhance the available bandwidth in wireless communication the use of multiple antennas at the receiving and the transmission side has become an important option [1]. In such multiple input multiple output (MIMO) systems it has been demonstrated that the scattering of the radio waves can lead to an increase of the effective bandwidth available for communication [2–5]. The best results for the channel capacity in MIMO systems are obtained in a strongly scattering environment, where direction and arrival time of the scattered signals is determined by diffusive propagation of the waves. The channel capacity can be severely limited by residual correlation between the channels even in a scattering environment. Strong correlations exist when the scattering is not sufficient to separate the individual connections between the $M\times N$ antennas [4]. This is, for example, the case when transmitter and receiver arrays are placed far apart from each other in an environment without scattering. An instructive example of the influence of correlation has been developed by Chizhik *et al.* [6] by modeling the scattering by diffractive keyholes in a screen between the transmitters and the receivers. When all the waves are forced to go through a single keyhole in the screen, all channels are fully correlated and the capacity remains low. From a physics point of view, the wireless communication problem has many aspects in common with topics from condensed matter physics such as light waves in strongly scattering media and electron transport in disordered conductors [4].

Estimating the capacity of data transfer in complex environments by measuring and modeling has become an important issue to optimize the positioning of base stations and receivers in a wireless network found in, e.g., cellular phone networks and wireless computer networks. Both the spatial, "speckle," and temporal characteristics, "fading," of the wave fields influence the available capacity. In many modern transceivers the actual encoding and decoding procedure of the signals is dynamically adapted to the changes in the environment. The capacity of data transfer in a MIMO system operating in a scattering medium is given in the generalized Shannon approach as [7,8]

$$C=\log_2 \det\left[\mathbf{I}+\frac{\rho}{M}\mathbf{H}^{\dagger}\cdot\mathbf{Q}\cdot\mathbf{H}\right], \tag{1}$$

in units of Bits per second per Hz bandwidth. Here $\mathbf{H}$ is the $M\times N$ channel coupling matrix between M transmitting and N receiving antennas. All the effects of the wave propagation, scattering, absorption, etc., are part of the matrix $\mathbf{H}$ and its transposed conjugate $\mathbf{H}^{\dagger}$. The other parameters in Eq. (1) are the parameter ρ describing the available electronic signal to noise ratio in the system for each transmitter, the covariance matrix $\mathbf{Q}$ defining the transmitted power distribution over the channels, and the unity matrix $\mathbf{I}$. An estimate of the channel capacity for a given configuration of transmitting and receiving antennas is obtained by measuring or calculating $\mathbf{H}$. A singular value analysis of $\mathbf{H}$ with non-negative solutions $S_i, i=1,\ldots,\min(N,M)$ gives the eigenvalues $\Lambda_i=S_i^2$ of $\mathbf{H}^{\dagger}\cdot\mathbf{H}$. Each eigenvalue specifies an independent communication channel.

The distribution of available transmitter power over the independent channels as specified by $\mathbf{Q}$ in Eq. (1) is still free to choose to maximize the data transfer capacity. For example, all power could be assigned to the channel with the largest singular value $S_{\max}$. In that case the determinant in Eq. (1) reduces to a single element: $\log_2(1+\rho/MS_{\max}^2)$. Without knowledge of the channel matrix an equal distribution of transmitter power over all available channels gives for the correlation matrix $\mathbf{Q}=\mathbf{I}$. With ρ sufficiently large, the determinant in Eq. (1) reduces in this case to a sum over Λ_i. An improvement in capacity can be obtained by using the available information about the channel strengths S_i and optimizing the choice for $\mathbf{Q}$ by, for example, the "water filling" method [9]. Knowledge about the distribution of singular values due to array geometry can assist in finding the optimum distribution of transmitter power.

The singular value distribution and the associated channel capacity in MIMO systems is studied here when the antennas in the transmitter and receiver arrays are regularly spaced. This problem has a strong similarity to the self-imaging of

*Electronic address: sprik@science.uva.nl; URL: http://www.science.uva.nl/wzi

 ©2005 The American Physical Society

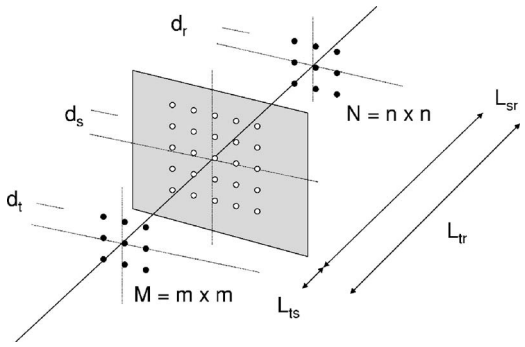

FIG. 1. The schematic diagram of a configuration with a $M=m\times m$ transmitter array with period d_t and $N=n\times n$ receiver array with a period d_r and distance L_{tr}. The intermediate screen at distance L_s transmits the waves only through the small holes.

diffraction gratings in optics. In 1836 Henry Fox Talbot [10] noticed that an illuminated grating with a periodicity d displays a sharp self-image at a large distance depending on the grating periodicity d and the wavelength λ. In 1881 Rayleigh showed that the self-imaging occurs at multiples of the distance: $L_{\mathrm{Talbot}}=2d^2/\lambda$ [11] and follows from the scalar diffraction theory in the Fresnel limit. At intermediate distances a modified replica is generated at rational fractions of L_{Talbot} [12,13] for gratings with a transmission $1/M$ with M an integer. The imaging effects occur at a distance between screen and array given by $L=(p/q+k/2)L_{\mathrm{Talbot}}$, with $p=0,1,2,\ldots$, $q=2,3,\ldots$, and $k=0,1,2,\ldots$. The phase and intensity distribution is in general more complicated than the image at integer distances [14]. The fractional Talbot effect has an intricate link with the mathematics of the infinite sums of Gaussian numbers as was outlined by Berry [12]. Recently the Talbot effect has been applied in self-imaging application without the need for external optical elements and is frequently used in composite diffractive optical elements such as lenslet arrays and beam splitters [15]. Similar imaging effects are also observed in the interference phenomena of quantum mechanical matter waves as so-called "quantum carpets" [13] and used in interferometry of cold atoms [16].

In the following sections it will be shown that the Talbot effect is also important in the data transfer capacity between antenna arrays. Figure 1 shows the schematic layout of the configuration used in the model calculation. The channel transfer matrix $\mathbf{H}$ between the arrays is modeled by using a three dimensional scalar free space Green's function $G_k(\vec{r}_1,\vec{r}_2)=e^{ikr}/4\pi r$ to calculate the wave propagation from point $\vec{r}_1$ to $\vec{r}_2$ with $r=\|\vec{r}_2-\vec{r}_1\|$ for a wave vector $k=2\pi/\lambda$ [17]. In the following the wave vector is chosen as $k=1$ and thus $\lambda=2\pi$ and is not explicitly listed further. In free space $\mathbf{H}_{ij}=G(\vec{r}_i,\vec{r}_j)$, with $\vec{r}_i$ and $\vec{r}_j$ the positions of transmitter i and receiver j. A singular value analysis of the matrix as [18] $\mathbf{H}=\mathbf{U}\cdot\mathbf{S}\cdot\mathbf{V}^{\dagger}$ provides the singular values S_i on the diagonal of $\mathbf{S}$ and the associated singular vectors as the columns of $\mathbf{U}$ for the transmitter and $\mathbf{V}$ for the receiver.

Figure 2 shows the results without an intermediate screen for a typical example using 3×3 transmitter and receiver arrays with $d_t=d_r=250$ and $L_{\mathrm{Talbot}}=2d_td_r/\lambda=1.989\times10^4$. Hence, $d_t,d_r\gg\lambda$. The horizontal axis shows the distance scaled to L_{Talbot}. The dominant singular value is strongly

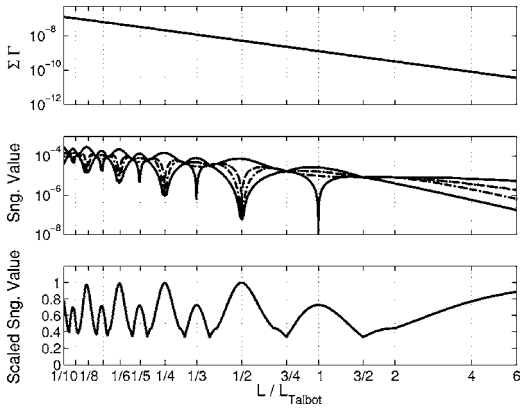

FIG. 2. Singular value analysis of a 3×3 receiver: 3×3 transmitter system as function of the distance between the arrays. The top graph shows the sum of all eigenvalues, the middle graph shows the first five largest singular values, and the bottom graph the dominant singular value scaled by $4\pi L_{\mathrm{rt}}/\sqrt{MN}$.

modulated as function of the distance with maxima near $L_{\mathrm{rt}}/L_{\mathrm{Talbot}}=1/2,1/4,1/6,\ldots$. The other singular values near these fractional distances vanish. The overall sum of the square of the singular values is a smooth function approaching a L_{tr}^{-2} dependence at larger distances. The scaling can be understood by considering the trace of $\mathbf{H}^{\dagger}\cdot\mathbf{H}$ which is the sum of the eigenvalues, but also the sum of the matrix elements: $\Sigma_{u=1\cdots N}\mathbf{H}^{\dagger}\cdot\mathbf{H}_{uu}=\Sigma_{i=1\cdots M,j=1\cdots N}1/(4\pi r_{ij})^2$ and scales with $MN/(4\pi L)^2$ at distances larger than the lateral dimensions of the arrays. Beyond $L_{\mathrm{tr}}\simeq L_{\mathrm{Talbot}}$ the modulations smooth out and the singular value approaches the asymptotic scale behavior.

The distribution of singular values for fractions of the Talbot distance can be understood using the paraxial approximation. Under these conditions it is assumed that the distance between the arrays L_{tr} is much larger than the distances between the elements i and j in the arrays. The distance $\vec{r}_i-\vec{r}_j$ in the paraxial approximation is given by $\|\vec{r}_i-\vec{r}_j\|=\sqrt{L_{\mathrm{tr}}^2+(x_i-x_j)^2+(y_i-y_j)^2}\simeq L_{\mathrm{tr}}(1+\delta^2n_x^2/2+\delta^2n_y^2/2)$, with n_x and n_y an integer indicating the distance between elements in the array in units of periodicity d_t, and $\delta=d_t/L_{\mathrm{tr}}$ the paraxial expansion parameter. The maximum value of n_x and n_y is determined by the lateral dimensions of the two arrays. With this approximation

$$\mathbf{H}_{ij}^{pa}\simeq\frac{e^{ikL_{\mathrm{tr}}}}{4\pi L_{\mathrm{tr}}}\frac{e^{i(kL_{\mathrm{tr}}/2)(\delta^2n_x^2+\delta^2n_y^2)}}{[1+\delta^2(n_x^2+n_y^2)]}\simeq\frac{e^{ikL_{\mathrm{tr}}}e^{i(kd_t^2/2L_{\mathrm{tr}})(n_x^2+n_y^2)}}{4\pi L_{\mathrm{tr}}}.$$

The matrix elements of $\mathbf{H}^{pa}$ become identical for any integer value n_x and n_y if $kd_t^2/2L_{\mathrm{tr}}$ is a multiple of 2π. This condition is fulfilled if $L_{\mathrm{Talbot}}/4L_{\mathrm{tr}}$ is an integer, where $L_{\mathrm{Talbot}}=2d_t^2/\lambda$ the Talbot distance as defined in the self-imaging problem. Then all matrix elements are identical to $e^{ikL_{\mathrm{tr}}}/4\pi L_{\mathrm{tr}}$ and only one nonzero singular value $\min(\mathrm{N},\mathrm{M})e^{ikL_{\mathrm{tr}}}/\pi L_{\mathrm{tr}}$ remains. This explains in particular the distribution of the singular values near the fractional distances at $L_{\mathrm{tr}}/L_{\mathrm{Talbot}}=1/4Z=1/4,1/8,1/16,\ldots$ with $Z=1,2,\ldots$. With further specification of the size and shape of the arrays, the effect on the singular values can be predicted in more detail. For example,

for two parallel one-dimensional linear arrays with $N=M$ matrix $\mathbf{H}^{pa}$ has a symmetric Toeplitz structure [19] with elements $\mathbf{H}^{pa}_{ij} \propto U^{|i-j|^2}$, where $U=e^{i2\pi L_{\mathrm{Talbot}}/4L_{\mathrm{tr}}}$. The matrix $\mathbf{H}^{pa}$ has zero valued singular values when the determinant of $\mathbf{H}^{pa}$ is zero. The analytical factorization of the determinant into prime polynomials of U [18] gives these values at the roots of the polynomials. The analysis shows in particular that the roots of $U\pm 1=0$ give fractional positions $1/4Z=1/4,1/8,1/16,\ldots$ and $1/(4Z+2)=1/2,1/6,1/10,\ldots$, where only one nonzero singular value exists. For the roots of other prime polynomials that occur: $U^2+1, U^2\pm U+1, U^4+1,\ldots$, a limited number of nonzero singular values exist. Crossed linear arrays have always a single dominant singular value. The analysis for the two-dimensional arrays give similar conditions on U for the single dominant singular values as can be seen in Fig. 2 at the root positions of $U\pm 1=0$. At positions $1,1/3,1/5,\ldots$ associated with the roots of U^2+1 only a limited number of nonzero singular values exist. There are also positions where all the singular values are equal. This position occurs at fractions of L_{Talbot} with locations that depend on the array geometry and size. For example, in Fig. 2 at position $3/4$ all singular values are equal. The complexity of the singular value spectrum is related to the fact that all elements in $\mathbf{H}^{pa}$ are of the form U^{Z^2}. For $U \propto e^{(2\pi ip/q)}$ with p and q integers, the mathematical properties of square residues and finite Gaussian sums, as studied, in number theory, for example, generate the intricate behavior of the singular value spectrum.

The capacity given by Eq. (1) follows from the singular value analysis and depends further on the signal to noise ρ and the signal distribution. For large enough ρ the capacity is mainly determined by the distribution of the Λ_i values and the particular choice for $\mathbf{Q}$. Some general limits for a $M\times N$ MIMO system have been studied to obtain bounds to the capacity [2]. In particular for large L_{tr} all the matrix elements in $\mathbf{H}$ approach $\mathbf{H}^{\infty}_{ij}=e^{ikL_{\mathrm{tr}}}/(4\pi L_{\mathrm{tr}})$. This limit matrix $\mathbf{H}^{\infty}$ has only one nonzero singular value $S^{\infty}=NM/(4\pi L_{\mathrm{rt}})$, which is identical to the limit of the dominant singular value shown in Fig. 2. The associated capacity $C_{\infty}=\log_2(1+N\rho)$ and is differs from the capacity: $C_{\mathbf{I}}=N\log_2(1+\rho/N)$ for parallel channels $\mathbf{H}=\mathbf{I_N}$.

The conditions used in Fig. 2 were chosen such that d and $L_{\mathrm{Talbot}} \gg \lambda$. If $d \simeq \lambda$ the modulation of the singular values is not occurring at exact fractions of the Talbot distance, but in general at shorter distances the closer the near-field conditions are approached. The calculated geometry is still well in the Fresnel diffraction limit as long as the aperture of the arrays is large with respect to the distance. In particular, the Talbot distance approaches the Fresnel number $F \simeq (nd_t)^2/\lambda L_{\mathrm{tr}}$ if $2d_t^2/\lambda \simeq (nd_t)^2/\lambda$, which is the case for only very small arrays. At $L_{\mathrm{tr}} > L_{\mathrm{Talbot}}$ the Fraunhofer diffraction limit is reached when F becomes small and the detailed structure in the singular value distribution is lost.

The results shown in Fig. 2 are for propagation of waves in free space. The apparent correlations between the channels are caused by the interference of all the participating transmitter antennas. Placing a screen with keyholes between the transmitter and the receiver (see Fig. 1) modifies the transfer [6]. The effect of the screen mimics communication through

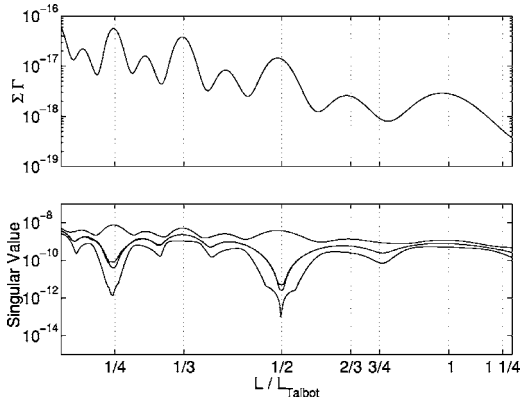

FIG. 3. Singular value analysis of a 3×3 receiver: 3×3 transmitter system through a screen with an array of keyholes as function of L_{sr} and $L_{\mathrm{ts}}=L_{\mathrm{Talbot}}$.

conduits or waveguides with a limited number of available paths for the waves. For a number of holes smaller than the number of antennas N and M in the arrays a strong correlation between channels remains. In particular for one hole on axis with a diameter much smaller than λ the correlation is the strongest. The channel matrix $\mathbf{H}$ is now calculated as $\mathbf{H}_{ij}=\Sigma_h G(\vec{r}_i,\vec{r}_h)G(\vec{r}_h,\vec{r}_j)\chi(\vec{r}_i,\vec{r}_h,\vec{r}_j)$ with $\vec{r}_h$ the position of hole h in the screen. The term $\chi(\vec{r}_i,\vec{r}_h,\vec{r}_j)$ depends on the angle between the incoming and outgoing direction and is determined by the boundary conditions on the diffraction screen [17]. If the type-I Rayleigh-Summerfeld diffraction integral is used, then $\chi=1$. Other choices add angular-dependent terms to each of the matrix elements. In particular for the conventional Fresnel-Kirchhoff approximation $\chi(\vec{r}_i,\vec{r}_h,\vec{r}_j)=\cos(\alpha)$ with α the angle between $(\vec{r}_h-\vec{r}_i)$ and $(\vec{r}_j-\vec{r}_h)$. By using a single screen, the waves are only scattered once and multiple scattering effects are suppressed. The model can easily be extended to include multiple scattering by using point-like scatterers instead of holes and treating the wave propagation, including all multiple scattering, in an exact T-matrix approach as is often done in condensed matter physics (see Ref. [20]).

It is illustrative to look at the basic case of 1 hole and $N=2$ to $M=2$ antenna configuration. The capacity can then explicitly be expanded as [21]

$$C_{2\times 2}=\log_2[1+\rho/2(\mathbf{R}_{11}+\mathbf{R}_{22})+(\rho/2)^2(1-|\mathbf{R}_{\mathrm{cor}}|)],$$

with $\mathbf{R}=\mathbf{H}^{\dagger}\cdot\mathbf{H}$ with elements

$$\mathbf{R}_{11}=|G(\vec{r}_{t1},\vec{r}_h)|^2|G(\vec{r}_h,\vec{r}_{r1})|^2,$$

$$\mathbf{R}_{12}=\mathbf{R}_{21}^{*},$$

$$=G(\vec{r}_{t1},\vec{r}_h)G^{*}(\vec{r}_{t2},\vec{r}_h)G(\vec{r}_h,\vec{r}_{r1})G^{*}(\vec{r}_h,\vec{r}_{r2}),$$

$$\mathbf{R}_{22}=|G(\vec{r}_{t2},\vec{r}_h)|^2|G(\vec{r}_h,\vec{r}_{r2})|^2,$$

and $|\mathbf{R}_{\mathrm{cor}}|^2=\mathbf{R}_{12}\mathbf{R}_{21}/|\mathbf{R}_{11}\mathbf{R}_{22}|$ the cross-correlation. All paths are forced through the single hole and the correlation becomes $|\mathbf{R}_{\mathrm{cor}}|=1$. Hence the second term in $C_{2\times 2}$ cancels and the channel capacity is considerably reduced for all positions

of the hole or the antennas. The remaining variations are due to the signal powers $\mathbf{R}_{11}$ and $\mathbf{R}_{22}$. In the general case of more antennas and holes the strong reduction remains observable. The dominant singular value is much larger than any of the other values over the whole range and fully determines the small total capacity in the system. Also the oscillations of the singular values near fractions of the Talbot distances are suppressed. Adding more holes in the screen increases the total transmitted power and influences the strong correlation between the channels. Figure 3 shows the results for a screen with a regular hole pattern matching the periodicity of the transmitter and the receiver arrays. The singular values again show strong variation near the fractional Talbot distances. The overall sum now shows a strong modulation at the fractional distances. Further calculations show that placing the screen or the receiver at an irrational distance reduces the overall modulation and capacity. Also choosing a random placement of the holes in the screen or of the antennas in the arrays reduces the modulation and the capacity.

In conclusion, wireless data transfer between periodic arrays is sensitive to the distance with the Talbot distance L_{Talbot} as the relevant length scale. At particular rational fractions of L_{Talbot} a single channel is dominant and carries all information. At other fractional distances all singular values are equal. After inserting a screen with a periodic array of holes, the Talbot type modulation are still present.

This work is part of the research programme of the Stichting voor Fundamenteel Onderzoek der Materie (FOM), which is financially supported by the Nederlandse Organisatie voor Wetenschappelijk Onderzoek (NWO).

[1] T. S. Rappaport, *Wireless Communications: Principles and Practice*, 2nd ed. (Prentice Hall, Upper Saddle River, NJ, 2002).
[2] G. J. Foschini and M. J. Gans, Wireless Personal Communications **6**, 311 (1998).
[3] A. L. Moustakas, H. U. Baranger, L. Balents, A. M. Sengupta, and S. H. Simon, Science **287**, 287 (2000).
[4] S. H. Simon, A. L. Moustakas, M. Stoytchev, and H. Safar, Phys. Today **54(9)**, 38 (2001).
[5] B. E. Henty and Daniel D. Stancil, Phys. Rev. Lett. **93**, 243904 (2004).
[6] D. Chizhik, G. Foschini, M. Gans, and R. Valenzuela, IEEE Trans. Commun. **1**, 361 (2002).
[7] E. Telatar, AT&T-Bell Technical Memorandum (1995, see: http://mars.bell-labs.com); Eur. Trans. Telecom. **10**, 585 (1999).
[8] C. E. Shannon, Bell Syst. Tech. J. **27**, 379 (1948).
[9] T. M. Cover and J. A. Thomas, *Elements of Information Theory* (John Wiley & Sons, New York, 1991).
[10] H. F. Talbot, Philos. Mag. **9**, 401 (1836).
[11] Lord Rayleigh, Philos. Mag. **11**, 196 (1881).
[12] M. V. Berry and S. Klein, J. Mod. Opt. **43**, 2139 (1996).
[13] M. Berry, I. Marzoli, and W. Schleich, Phys. World **june**, 39 (2001).
[14] H. Wang, C. Zhou, and L. Liu, Opt. Commun. **173**, 17 (2000).
[15] K. Patorski, in *Progress in Optics*, edited by E. Wolf (North Holland, Amsterdam, 1989), Vol. 27, p. 3–108.
[16] J. F. Clauser and S. Li, Phys. Rev. A **49**, R2213 (1994).
[17] J. D. Jackson, *Classical Electrodynamics* (Wiley Publications, New York, 1962).
[18] Numerical calculations performed with Matlab: http://www.mathworks.com and analytical manipulations with Mathematica: http://www.wolfram.com.
[19] W. H. Press, B. P. Flannery, S. A. Teukolsky, and W. T. Vetterling, *Numerical Recipes in FORTRAN*, 2nd ed. (Cambridge University Press, Cambridge, England, 1992).
[20] R. Sprik, *Physical Modelling of a Dispersed Multi Channel System*, Proceeding of the 13th IST Mobile and Wireless Communications Summit, 28–30 June 2004, Lyon, France (unpublished).
[21] S. Loyka and A. Kouki, IEEE Trans. Commun. **50**, 1886 (2002).